Sensitivity of photonic crystal fiber grating sensors: biosensing, refractive index, strain, and temperature sensing

Lars Rindorf and Ole Bang
COM•DTU, Department of Communications, Optics and Materials, Technical University of Denmark, DK-2800 Kgs. Lyngby, Denmark

We study the sensitivity of fiber grating sensors in the applications of strain, temperature, internal label-free biosensing, and internal refractive index sensing. It is shown that optical dispersion plays a central role in determining the sensitivity, and the dispersion may enhance or suppress sensitivity as well as change the sign of the resonant wavelength shifts. We propose a quality factor, Q, for characterizing LPGs.

OCIS codes:

1. Introduction

Optical fiber grating sensors are becoming increasingly widespread in a wide range of applications[1]. Their characteristics include immunity to electromagnetic interference, high sensitivity, fast response, and keeping their calibration with time. Furthermore they possess a high tolerance to harsh environments such as sea water, concrete, and extreme temperatures. The measured parameter, the resonant wavelength of the grating, is usually linear in the magnitude of the measurand, e.g. temperature or strain, allowing for an accurate quantitative estimate of the measurand.

Photonic crystal fibers (PCFs)[2] are optical fibers, in which the cladding consists of a microstructured array of air holes running along the fiber axis. Here we consider index guiding PCFs, which have a solid core in the form of a missing air hole in the center. In index guiding PCFs light is confined to the core by modified total internal reflection, analogous to guiding in standard optical fibers. The holes in the cladding are most commonly placed in a periodic triangular structure, which is characterized by a lattice constant (pitch) and the diameter of the holes. PCFs are typically made of silica[2] or, more recently, polymer materials, where they are termed microstructured polymer optical fibers (mPOFs)[3]. The hole structure in the cladding determines the optical properties of the PCF, which allows for a large degree of freedom in tayloring key properties, such as dispersion and group velocity.

In standard optical fibers the silica in the core contains dopants to increase the refractive index. The refractive index of the doped silica is sensitive to UV radiation and this may be used for inscription of gratings. This technique can not be used for pure silica PCFs, since the core is not UV sensitive. For long-period gratings (LPGs) in PCFs other techniques exist, such as using an electric arc[4], a CO_2 laser[5], or mechanical microdeformation[6]. Otherwise the PCF can be specially made with a UV sensitive core for fiber gratings allowing for the inscription of both LPGs and Bragg gratings (BGs)[7].

Polymer has a smaller Young's modulus and greater elastic limit than silica, which makes it a good material for measuring strain and bending. In addition, polymer is biocompatible and can bind biomolecules directly to its surface, making it ideal for biosensing. Standard polymer optical fibers are made of poly-methyl methacrylate (PMMA), which is inherently photosensitive, allowing for both BGs[8] and LPGs[9] to be inscribed using a UV lamp. The inherent UV sensitivity was also recently used to write BGs in mPOF[10], whereas heat treatment under mechanical stress was used to write the first permanent LPG in an mPOF[11].

An important property of grating sensors in silica PCFs are that they are largely temperature insensitive, showing ~ 1 pm/K for both BGs[12] and LPGs[13]. The strain sensitivity is of the same order for LPGs and BGs in PCFs, and thus strain sensors may be realized with reduced cross sensitivity to temperature sensing. In addition, the holes of a PCF can be infiltrated with a substance having a high temperature coefficient to reduce or enhance the temperature sensitivity[14].

Whereas fiber-optic strain and temperature sensors use the material properties of the fiber, fiber-optic biosensors and refractive index sensors use the principle of evanescent wave sensing. In particular, there is a growing interest in optical biochemical sensors[15]. Here PCFs have the advantage that the analyte may be infiltrated into the air holes and thereby create a strong interaction with the probing electromagnetic field[16,17]. When using mPOFs one can take advantage of different polymers with special biosensing properties, such as TOPAS[18].

Liquid infiltrated PCF-LPGs[19,20] and PCF-BGs[14,21] have been demonstrated, which is an important step towards the ultimate goal of developing a so-called *label-free* biosensor in a PCF. Fiber gratings potentially allow for label-free biosensing with PCFs[20] by tracking how the grating resonance changes during operation. This may open for new possibilities in biomedical applications[22].

The dispersion plays a crucial role for all types of grating sensors in standard optical fibers[23,24]. The dispersion of PCFs depends strongly on the hole structure in the

cladding and thus the performance of the PCF grating sensor can be designed by an appropriate choice of pitch and hole size.

In this paper we explore the possibility of optimizing the hole structure of PCFs for sensing purposes. We do this by analyzing the sensitivity of triangular PCF gratings for different pitch and hole diameters. The applications under study are biosensing, refractive index sensing, strain, and temperature sensing. We show that the sensitivity is strongly influenced by the choice of the structural parameters of the PCF. We employ realistic values for the fibers parameters and give realistic values of pitch and hole diameter that minimize or maximize the sensitivity to different measurands.

We find that BGs are best characterized in the usual way by their sensitivity, γ, defined as the resonant wavelength shift divided by the resonant wavelength. In contrast, we find that the LPGs are best characterized by their quality factor, Q, defined as the resonant wavelength shift divided by the full-width at half maximum (FWHM) of the resonance dip.

2. Photonic crystal fibers

The eigenmodes of the PCFs for a temporally harmonic electrical field, $\mathbf{E}(\mathbf{r},t) = \mathbf{E}_\omega(\mathbf{r})e^{-i\omega t}$, may be found from Helmholtz eigenvalue equation,

$$\nabla \times \nabla \times \mathbf{E}_\omega(\mathbf{r}_\perp, z) = \frac{\omega^2}{\mathrm{c}^2}\varepsilon(\mathbf{r}_\perp)\mathbf{E}_\omega(\mathbf{r}_\perp, z), \qquad (1)$$

where ω is the angular frequency, c is the speed of light in vacuum, ε is the dielectric function, and $\mathbf{r}_\perp = (x, y)$ is the transverse coordinate vector. The z-axis is chosen to coincide with the fiber axis. We look for plane-wave solutions of the form $\mathbf{E}_\omega(\mathbf{r}) = \mathbf{E}_\omega(\mathbf{r}_\perp)e^{i\beta z}$ with β being the propagation constant. The effective index is defined as $n_{\mathrm{eff}}(k) = \beta(k)/k$, where k is the free-space wavevector and is related to the frequency and wavelength by $k = \omega/\mathrm{c} = 2\pi/\lambda$. The effective indices of the core mode and a resonant cladding mode are denoted by n_{co} and n_{cl}. The orthonormalization for Eq. (1) is

$$\int_\Omega \mathrm{d}\mathbf{r}_\perp \mathbf{E}_m^\dagger(\mathbf{r}_\perp)\varepsilon(\mathbf{r}_\perp)\mathbf{E}_n^\dagger(\mathbf{r}_\perp) = \delta_{mn}. \qquad (2)$$

The PCF is typically made of two materials with a high refractive index contrast. A general dielectric function, $\varepsilon(\mathbf{r})$, for a two material triangular PCF structure is described by high and low index regions as seen in Fig. 1. The periodic triangular structure is spanned by the lattice vectors $R_1 = (\sqrt{3}, 1)/2$ and $R_2 = (\sqrt{3}, -1)/2$. The general dielectric function equals n_b^2 for the base region and n_h^2 for the hole regions, with n_b and n_h being the refractive indices of the base and hole material, respectively.

The effective index of the core depends strongly on the wavelength, the hole diameter, and the pitch. The hole diameter, d, and pitch, Λ, are indicated in Fig. 1. Large hole diameters and small pitch also give a small core and therefore a strong effective nonlinearity.

Triangular silica PCFs are single mode for $d/\Lambda < 0.42$ for all wavelengths [25,26]. For small hole sizes ($d/\Lambda < 0.3$) the PCF is only weakly guiding, and bend losses increase drastically. Bend losses also become pronounced in the short wavelength limit, $\lambda \ll \Lambda$, regardless of hole diameter. PCFs can be designed to have a large mode area.

The transmission spectrum of an LPG in a PCF only shows a few cladding mode resonances, whereas several resonances are seen in a standard optical fiber LPG spectrum. The cladding modes of a PCF are different from the cladding modes of a standard optical fiber, since the fiber cross sections obey very different symmetries. In particular a PCF obeys a six-fold rotational symmetry (C_6^v) while the standard optical fiber has circular symmetry. The effective indices of the cladding modes of a PCF are closely spaced, and this spacing is much smaller than the difference between the core effective index and the effective index of any cladding mode. In other words, the beat length between any two cladding modes is much longer than the beat length between a cladding mode and the core mode. In practice we can assume $n_{\mathrm{cl}} \simeq n_{\mathrm{FSM}}$ for all cladding modes, where the fundamental space filling mode, n_{FSM}, is the effective index of an infinite cladding structure spanned by the lattice vectors in Fig. 1.

We have calculated the effective index for the core mode, n_{co}, and the fundamental space filling mode, n_{FSM}, for different hole to pitch and wavelength to pitch ratios, with the base material having a refractive index 1.45, which is the refractive index of silica at the wavelength $\lambda \simeq 1\mu$m. The effective indices are shown in Fig 2. The effective indices decrease with increasing hole size (d/Λ) or increasing normalized wavelength (λ/Λ). The effective index of the core mode is larger than that of the FSM, regardless of the fiber structure parameters (d,Λ).

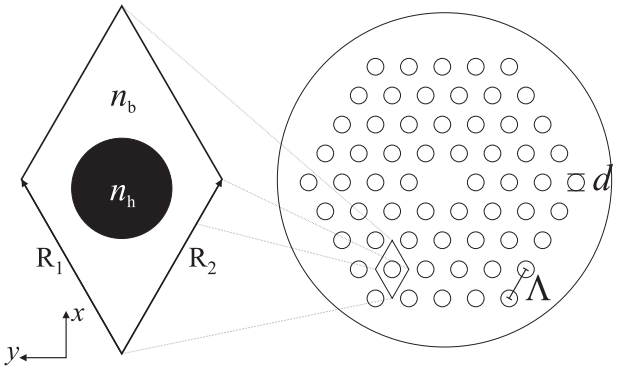

Fig. 1. A PCF with triangular cladding structure. The structure is characterized by the lattice vectors, R_1 and R_2, the hole size, d, and the pitch, Λ. The refractive indices n_h and n_b are the hole and base material refractive indices

3. Coupled mode theory

A. Introduction

Coupled mode theory[27] is a simple and compact theory that has been successful in accounting for the characteristics of fiber gratings. It allows us to derive the qualitative behavior of the gratings with some general, simplifying assumptions on the physical mechanisms. The theory assumes that near resonance the electromagnetic field propagating through the fiber may be expressed as a superposition of eigenmodes of the unperturbed fiber $a_{\rm co}(z)\mathbf{E}_{\rm co}(\mathbf{r}_\perp)e^{i\beta_{\rm co}z} + a_i(z)\mathbf{E}_i(\mathbf{r}_\perp)e^{i\beta_i z}$, where '$i$' denotes a resonant mode, and the a's are amplitude coefficients that depend on z due to the perturbation. For Bragg gratings the resonant mode is the counter propagating core mode, and for long-period gratings the resonant mode is a copropagating higher order mode, usually a cladding mode. The coupled-mode equations constitute a set of linear coupled differential equations. They may be expressed in a compact matrix form as

$$\begin{bmatrix} \frac{\partial a_{\rm co}(z,\delta_i)}{\partial z} \\ \frac{\partial a_i(z,\delta_i)}{\partial z} \end{bmatrix} = -i \begin{bmatrix} 0 & \kappa_i e^{i\delta_i z} \\ \kappa_i^* e^{-i\delta_i z} & 0 \end{bmatrix} \begin{bmatrix} a_{\rm co}(z,\delta_i) \\ a_i(z,\delta_i) \end{bmatrix} \quad (3)$$

where the detuning in the resonance between the core mode and the resonant mode, i, is

$$\delta_i \equiv \beta_{\rm co} - \beta_i - \frac{2\pi}{\Lambda_{\rm G}} \quad (4)$$

and the coupling constant is

$$\kappa_i = \frac{k^2}{2\sqrt{|\beta_{\rm co}\beta_{\rm i}|}} \int_\Omega d\mathbf{r}_\perp \mathbf{E}^\dagger_{\rm co}(\mathbf{r}_\perp)\Delta\tilde{\varepsilon}\big(\mathbf{r}_\perp\big)\mathbf{E}_i(\mathbf{r}_\perp), \quad (5)$$

where the integration is over the fiber cross section, Ω. $\Delta\tilde{\varepsilon}\big(\mathbf{r}_\perp\big)$ is the first phase matched Fourier component (± 1) in the expansion $\Delta\varepsilon(\mathbf{r}_\perp, z) = \sum_{m=-\infty}^{\infty} \Delta\tilde{\varepsilon}_m(\mathbf{r}_\perp)\exp(-im\frac{2\pi}{\Lambda_{\rm G}}z)$.

In Eq. (3) we have neglected the diagonal terms, the so called self-coupling terms. The self-coupling arises from the perturbation of the individual modes due to the index change of the grating. The self-coupling shifts the resonant wavelength some nm's, while otherwise leaving the spectrum of the grating unaltered. Since this effect is typically small we neglect it for our purposes.

Using Eq. (4) we obtain a resonance condition in terms of effective indices and the wavelength

$$\begin{aligned} \lambda_{\rm r} &= \big(n_{\rm co}(\lambda_{\rm r}) - n_i(\lambda_{\rm r})\big)\Lambda_{\rm G} \\ &\equiv \bar{n}_{\rm f}(\lambda_{\rm r})\Lambda_{\rm G}, \end{aligned} \quad (6)$$

where n_i is the effective index of the resonant mode. The equation is valid both for LPGs, $\bar{n}_{\rm f} = n_{\rm co} - n_{\rm cl}$, and BGs, $\bar{n}_{\rm f} = 2\, n_{\rm co}$.

In the following we use the bar for indicating a difference between the core and the resonant modes as done in Eq. (6). Thus $\bar{\beta} \equiv \beta_{\rm co} - \beta_i$ for the propagation constant, and for the group index we have $\frac{\partial\bar{\beta}}{\partial k} = n_{{\rm g,co}} - n_{{\rm g},i} \equiv \bar{n}_{\rm g} = -\lambda^2\partial_\lambda(1/L_B)$, where $L_B = 2\pi/\bar{\beta}$ is the beat length, with $n_{{\rm g},i} \equiv \frac{\partial\beta_i}{\partial k}$.

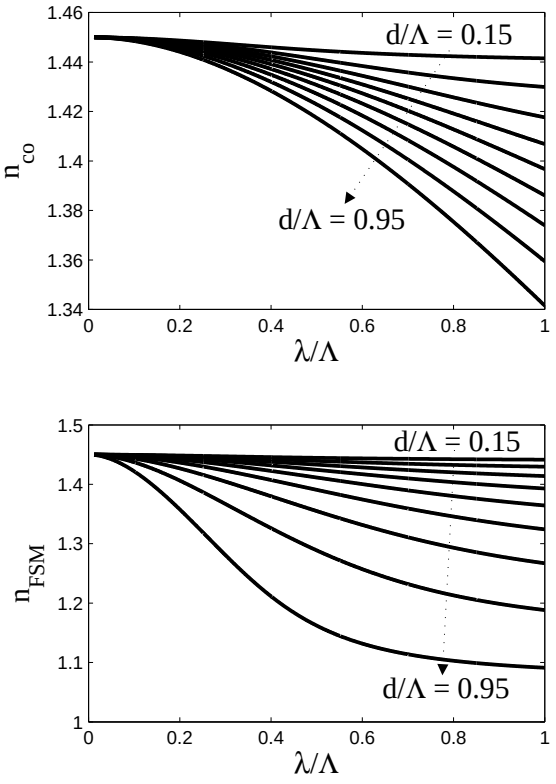

Fig. 2. Effective indices for the core (top) and fundamental space filling mode (FSM) modes for triangular photonic crystal fibers. The lines indicate different values of the hole diameter relative to the pitch. The lines correspond to different values of d/Λ, increasing by 0.1

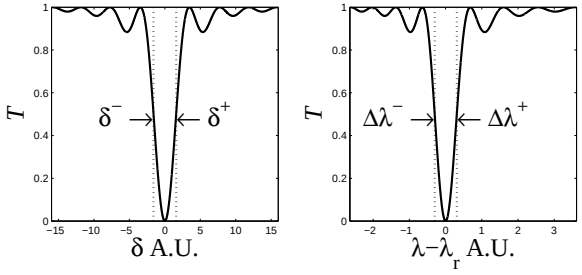

Fig. 3. Definition of the full-width half maximum (FWHM) in detuning, $\delta_{\rm FWHM} = \delta^+ - \delta^-$, and in wavelength, $\lambda_{\rm FWHM} = \Delta\lambda^+ - \Delta\lambda^-$.

The resonance conditions must be solved considering the dispersion of the effective indices, since these are strongly dependent on the pitch and hole size of the PCF structure as seen in Fig. 2.

B. Dispersion effects on the wavelength FWHM

Couple-mode theory in the form of Eq. (3) will give an expression for the transmission in terms of the detuning and coupling constant. However, experimentally the transmission is measured as function of wavelength.

In Fig. 3 the FWHM for the detuning, $\delta_{\mathrm{FWHM}} = |\delta^+ - \delta^-|$, and the wavelength, $\lambda_{\mathrm{FWHM}} = |\Delta\lambda^+ - \Delta\lambda^-|$, are

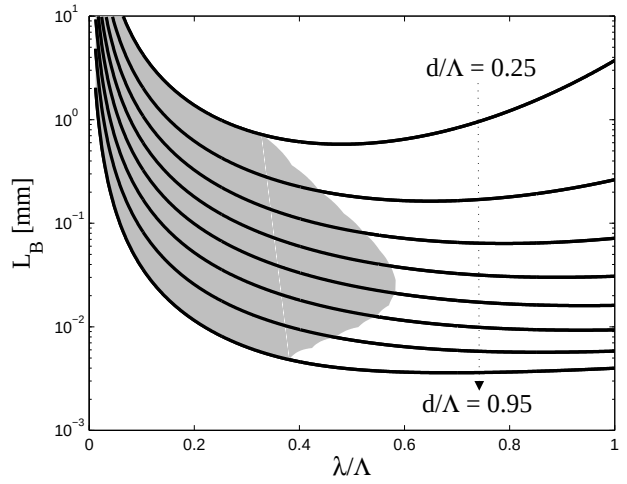

Fig. 4. Beat length as function of the wavelength over pitch, λ/Λ, for an LPG. The gray area indicates negative group index mismatch $\bar{n}_{\mathrm{g}} < 0$

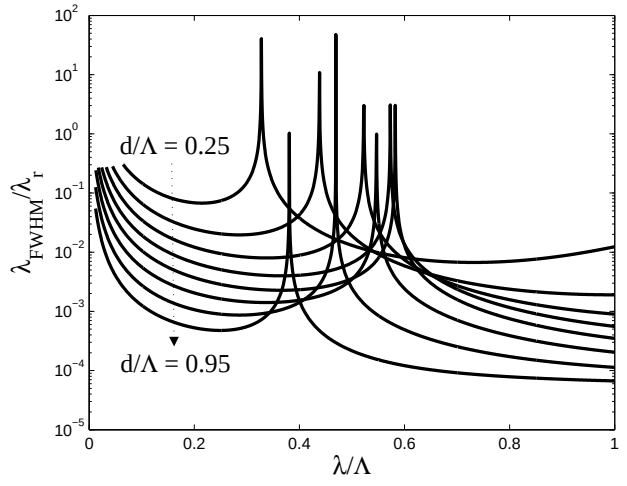

Fig. 5. FWHM as function of the wavelength over pitch, λ/Λ for an LPG

defined. By definition we have $T(\delta^+) = T(\delta^-) = 0.5$, and equivalently for the wavelength we have $T(\lambda_{\mathrm{r}} + \Delta\lambda^+) = T(\lambda_{\mathrm{r}} + \Delta\lambda^-) = 0.5$.

To find a relation between δ_{FWHM} and λ_{FWHM} that incorporates the dispersion of the effective indices we expand the detuning around the resonance wavelength to first order in $\Delta\lambda$

$$\begin{aligned}\delta(\lambda_{\mathrm{r}} + \Delta\lambda) &= \beta_{\mathrm{co}}(\lambda_{\mathrm{r}} + \Delta\lambda) - \beta_i(\lambda_{\mathrm{r}} + \Delta\lambda) - \frac{2\pi}{\Lambda_{\mathrm{G}}} \\ &\simeq \frac{\partial\bar{\beta}}{\partial k}\frac{\partial k}{\partial\lambda}\Big|_{\lambda_{\mathrm{r}}}\Delta\lambda = -\bar{n}_{\mathrm{g}}(\lambda_{\mathrm{r}})\frac{2\pi}{\lambda_{\mathrm{r}}^2}\Delta\lambda, \qquad (7)\end{aligned}$$

With this equation it is possible to obtain two equations relating δ^+ and δ^- to $\Delta\lambda^+$ and $\Delta\lambda^-$. Subtracting the two equations and taking the absolute value of both sides, we obtain an expression for δ_{FWHM} and λ_{FWHM}

$$\frac{\lambda_{\mathrm{FWHM}}}{\lambda_{\mathrm{r}}} = \frac{1}{2\pi}\frac{\lambda_{\mathrm{r}}\delta_{\mathrm{FWHM}}}{|\bar{n}_{\mathrm{g}}(\lambda_r)|}, \qquad (8)$$

which incorporates the dispersion of the effective indices in a consistent manner.

We note that the expression is not valid at group index matching between the two resonant modes, $\bar{n}_{\mathrm{g}} = 0$. In this limit, however, the FWHM goes to infinity, and any wavelength shifts of the sensor will become difficult to detect.

C. Long-period gratings

Long-period gratings couple the core mode to a co-propagating high-order mode. The difference in effective index of two such modes is typically small, hence by Eq. (6) the grating period of such a grating must be long, $\Lambda_{\mathrm{G}} \sim 100 - 1000 \times \lambda$. For LPGs we put the subscript i = FSM, and $a_i = a_{\mathrm{FSM}}, \delta = \delta_i = \delta_{\mathrm{FSM}}, \kappa = \kappa_i = \kappa_{\mathrm{FSM}}$

Typically the FWHM of an LPG is of the order of nanometers. The minimal detectable shift in resonance condition is thus set by the FWHM and not the spectral resolution of the spectrum analyzer.

The coupled-mode equations for the long-period grating may be solved analytically from Eq. (3) yielding the transmission coefficient

$$T(\delta) = 1 - \frac{1}{1 + \frac{\delta^2}{4|\kappa|^2}}\sin^2\left(|\kappa|L\sqrt{1 + \frac{\delta^2}{4|\kappa|^2}}\right). \qquad (9)$$

At resonance ($\delta = 0$) the transmission is sinusoidal, $T(\delta = 0) = \cos^2(|\kappa|L)$, where L is the length of the grating. The first zero for T is at $|\kappa|L = \pi/2$. Ignoring the wavelength dependence of the coupling constant, $\kappa = \kappa(\lambda_{\mathrm{r}}) = \pi/(2L)$, we substitute $\xi = \delta/(2|\kappa|)$ and solve $T(\xi) = 0.5$ numerically. This yields $\xi^+ = -\xi^- \simeq 0.80$. We can find the FWHM of the detuning as $\delta_{\mathrm{FWHM}}/|\kappa| = 2(\xi^+ - \xi^-) \simeq 3.2$. The wavelength FWHM of the transmission can then be found using Eq. (8)

$$\frac{\lambda_{\mathrm{FWHM}}}{\lambda_{\mathrm{r}}} \simeq 0.80\frac{1}{|\bar{n}_{\mathrm{g}}(\lambda_{\mathrm{r}})|}\frac{\lambda_{\mathrm{r}}}{L}. \qquad (10)$$

The wavelength FWHM obviously is large when the group index matching is close to zero, $\bar{n}_{\rm g}(\lambda_{\rm r}) = 0$.

In conclusion we have found an expression, characteristic for LPGs, that relates $\lambda_{\rm FWHM}$ directly with the length of the grating, the group index and the resonant wavelength. The expression is derived under the assumption, that $|\kappa(\lambda)L = \pi/2$

D. Bragg gratings

Bragg gratings couple the incident core mode to a counter-propagating core mode, hence $\beta_i = -\beta_{\rm co}$ and the effective index is $n_i = n_{\rm co}$ and the coupling constant $\kappa = \kappa_i = \kappa_{\rm co}$. From Eq. (6) we find that the period of such a grating must be comparable with the wavelength, $\Lambda_{\rm G} \sim \lambda/2$. The FWHM of a BG is usually very narrow compared with an LPG. Although a narrow FWHM gives a high resolution for a sensor, it also puts high demands on production tolerances and the optical spectrum analyzer. Thus the minimal detectable shift in the resonant wavelength is set by the spectrum analyzer.

Fluctuations in the effective index caused by imperfections in the PCF structure or the grating period along the grating enters by Eq. (6) in the transmission spectrum and can inflict a significant broadening of the resonance peak[21]. On the beneficial side one need only to couple light into one end of the PCF, since it is possible to measure the reflection spectrum of the grating.

The coupled-mode equations for the Bragg grating may be solved analytically from Eq. (3) yielding a transmission coefficient

$$T(\delta) = 1 - \frac{\sinh^2\left(|\kappa|L\sqrt{1-\frac{\delta^2}{4|\kappa|^2}}\right)}{\cosh^2\left(|\kappa|L\sqrt{1-\frac{\delta^2}{4|\kappa|^2}}\right) - \frac{\delta^2}{4|\kappa|^2}}. \qquad (11)$$

At resonance the transmission is equal to $T(0) = 1 - \tanh^2(|\kappa|L)$. Assuming that the coupling constant is constant, $\kappa = \kappa(\lambda_{\rm r})$, we find numerically that the $\delta_{\rm FWHM}$ can be approximated reasonably well by

$$\delta_{\rm FWHM} \simeq \frac{4.0|\kappa|L + 3.4}{L}. \qquad (12)$$

According to this estimate the FWHM decreases with the grating length until a lower bound set by the coupling strength itself.

Typically $|\kappa|L > 1$ and we can neglect the second term in Eq. (12) and obtain $\delta_{\rm FWHM} \simeq 4|\kappa|$. The wavelength FWHM is then

$$\frac{\lambda_{\rm FWHM}}{\lambda_{\rm r}} \;\simeq\; 0.64\frac{\lambda_{\rm r}|\kappa|}{|\bar{n}_{\rm g}(\lambda_{\rm r})|}. \qquad (13)$$

We note that the FWHM generally increases with the resonance wavelength squared.

In conclusion we have found an expression, characteristic for BGs, that relates $\lambda_{\rm FWHM}$ directly with the coupling constant, the group index of the core mode and resonant wavelength. We have made the assumption the coupling constant is independent of wavelength.

4. Linear response theory for fiber sensors

The fiber sensor is perturbed by a measurand to produce a change in the measured quantity, in our case the resonant wavelength. For quantitative and qualitative estimation of the measurand a linear relation to the resonant wavelength is assumed. Since the resonant wavelength shifts are generally small compared to the wavelength, it is natural to employ perturbation theory and Taylor expand the resonance condition to first order around the resonance wavelength.

Consider a general measurand, α. We assume that the shift in resonant wavelength as well as in the measurand are sufficiently small, and we expand the resonance condition Eq. (6) in the resonant wavelength and the measurand to first order

$$\lambda_{\rm r} + \Delta\lambda_{\rm r} = \Big[\bar{n}_{\rm f}(\lambda_{\rm r},\alpha) + \frac{\partial\bar{n}_{\rm f}}{\partial\lambda_{\rm r}}\Delta\lambda_{\rm r} + \frac{\partial\bar{n}_{\rm f}}{\partial\alpha}\Delta\alpha\Big]\Lambda_{\rm G}. \qquad (14)$$

Identifying $\Lambda_{\rm G} \equiv \lambda_{\rm r}/\bar{n}_{\rm f}(\lambda_{\rm r})$ by Eq. (6) and $\bar{n}_{\rm g} = \bar{n}_{\rm f} - \lambda\frac{{\rm d}\bar{n}_{\rm f}}{{\rm d}\lambda}$, we obtain an expression for the sensitivity

$$\begin{aligned}\gamma \;&=\; \Big|\frac{1}{\lambda_{\rm r}}\frac{{\rm d}\lambda_{\rm r}}{{\rm d}\alpha}\Big| = \Big|\frac{1}{\bar{n}_{\rm g}(\lambda_{\rm r})}\frac{\partial\bar{n}_{\rm f}}{\partial\alpha}\Big| \\ &=\; \begin{cases} \frac{1}{|n_{\rm g,co}-n_{\rm g,cl}|}\Big|\frac{\partial(n_{\rm co}-n_{\rm cl})}{\partial\alpha}\Big|, & \text{LPG}, \\ \frac{1}{|n_{\rm g,co}|}\Big|\frac{\partial n_{\rm co}}{\partial\alpha}\Big|, & \text{BG}. \end{cases}\end{aligned} \qquad (15)$$

The shift in the resonant wavelength is thus dependent on the change in the difference of the effective indices relative to the difference in group indices. We have chosen the symbol 'γ' for the sensitivity to match the notation of Shu et al.[28]. Obviously, when $|\gamma|$ is large the sensor will give large wavelength shifts, which will give a high sensitivity and accuracy of the measurand. However, changing the fiber parameters not only changes the wavelength shifts but also change the full-width half maximum (FWHM) of the resonance dip. Thus, even though $|\gamma|$ may be large for a certain fiber structure, the wavelength shifts will be difficult to detect if they are much smaller than the FWHM of the resonance dip. In particular, we therefore note that the sensitivity is high close to group index matching, $\bar{n}_{\rm g} = 0$, which by Eqs. (10,13) is also where the FWHM is wide. We introduce the quality factor, Q, of the grating sensor, which is the wavelength shift divided by the FWHM,

$$\begin{aligned} Q \;&=\; \frac{1}{\lambda_{\rm FWHM}}\frac{{\rm d}\lambda_{\rm r}}{{\rm d}\alpha} \\ &\simeq\; \begin{cases} \frac{1}{0.80}\frac{L}{\lambda_{\rm r}}\frac{\partial(n_{\rm co}-n_{\rm cl})}{\partial\alpha}, & \text{LPG}, \\ \frac{1}{0.64}\frac{1}{\lambda_{\rm r}|\kappa|}\frac{\partial n_{\rm co}}{\partial\alpha}, & \text{BG}. \end{cases}\end{aligned} \qquad (16)$$

We note that Q, in contrast to γ, does not increase when $\bar{n}_{\rm g} \to 0$. Perfect group index matching $\bar{n}_{\rm g} = 0$ only occurs for LPGs, as we will see in the following.

We have derived two expressions for the performance of a fiber grating sensor. The sensitivity, γ, is inversely

proportional to the group index mismatch, $\bar{n}_{\rm g}$, and expresses the shift in the resonant wavelength relative to the resonant wavelength. The quality factor, Q, in contrast, expresses the wavelength shift relative to the FWHM. Ideally both the sensitivity, γ, *and* the quality factor, Q, should be large.

The FWHM of LPGs is usually larger than the resolution of the spectrum analyzer. The quality factor is thus the most important measure of the performance of LPGs. The FWHM of BGs is usually narrow, and comparable to the resolution of the spectrum analyzer. The sensitivity is then the most important for BGs.

5. Numerical simulations

A. *Effective indices*

We employ a commercial finite element code (Comsol Multiphysics[29]) for the calculation of the effective indices. The code uses an adaptive mesh algorithm for generating the mesh. The meshes consist of 60,000-250,000 quadratical Lagrange elements. The core mode is simulated by considering a cross section with 12-25 rings of air holes: 12 rings for $d/\Lambda = 0.80 - 0.95$, 15 rings for $d/\Lambda = 0.50 - 0.75$, and 25 rings for $d/\Lambda = 0.15 - 0.45$. Outside the rings of air holes there is a layer of air 0.5Λ thick to reduce the effects of a finite cladding. The large number of rings of air holes is chosen such that effects of a finite cladding is small. Otherwise reflections may arise from both the silica-air interface and the metallic boundary outside the air layer. This induces an error on the effective index. In our simulation the number of rings was sufficiently large that the relative error on the effective indices is smaller than 10^{-4}. Large holes give a strong confinement of the core mode, and obviously fewer rings are needed compared to small holes.

We generally use only data where $n_{\rm co} - n_{\rm FSM} > 10^{-4}$ such that the error is negligible. This also makes physical sense, since the PCF is only weakly guiding below this limit.

For the fundamental space filling mode we use the Bloch theorem and we need only to simulate a single unit cell containing only one hole. The unit cell is spanned by the lattice vectors seen in Fig. (1) of an infinite triangular cladding structure. We impose periodic boundary conditions on the unit cell.

In our simulations we solve Eq. (1) for the propagation constants, β, for the modes of the fiber at a fixed frequency, ω, which enables us to include material dispersion in a consistent manner. For the refractive indices of the materials we use a Sellmeier expression for the silica and use the refractive index of water given in Ref.[30]. All plots in the following are shown as function of the wavelength relative to the pitch, but at a fixed wavelength. If the material dispersion is neglected then space and time in Maxwell's equation may be scaled with the pitch of the PCF. However, in our study the material dispersion cannot be neglected. We thus choose a wavelength $\lambda = 1.0\mu$m.

The grating period and therefore the beat length for LPGs can be determined from the effective indices using Eq. (6). The beat length varies significantly with the hole size and pitch, as shown in Fig. 4. The resonance condition, Eq. (6), can be satisfied over a range of wavelengths if $\partial_\lambda \Lambda_{\rm G} = 0$. For these values the FWHM of an LPG is very large.

The between the curves of in Fig. 4 the gray area indicates $\bar{n}_{\rm g} < 0$ and the white area $\bar{n}_{\rm g} > 0$. The boundary between these two areas indicates $\bar{n}_{\rm g} = 0$.

When the slopes of the curves in Fig. 4 are parallel with the normalized wavelength axis the resonance condition Eq. 6 is nearly matched for multiple normalized wavelengths, λ/Λ, we may thus expect that the wavelength FWHM is wide. By Eq. (8) the FWHM is widest when $\bar{n}_{\rm g} = 0$, indicated by the boundary of the gray area. It may seem surprising that the $\bar{n}_{\rm g} = 0$ does not coincide with zero slope of the curves. The curves in Fig. 4, however, are evaluated for a fixed wavelength with a variable pitch, and not for a fixed pitch with variable wavelength. The difference in normalized wavelength for group index matching and for zero slope of the curves is caused by material dispersion of silica.

For BGs $\bar{n}_{\rm f}$ in the resonance condition Eq. (6) only varies a few percent for all wavelengths, pitch values, and hole sizes. Thus the dispersion effects on the resonance condition are small. Correspondingly, it can shown that dispersion effects on the wavelength FWHM is also small, because the group index mismatch, $\bar{n}_{\rm g}$, in Eq. (8) only varies slightly ($< 12\%$) for index guiding PCFs, since $n_{\rm co}$ always dominates over its derivative in the group index, $n_{\rm g,co} = n_{\rm co} - \lambda \partial_\lambda n_{\rm co}$.

There is a fundamental difference between PCFs and standard optical fibers is that a PCF consists of two, often very different, materials. Standard optical fibers also consist of two materials: pure silica and a core of doped silica. In practice, however, the material parameters for the doped silica may often, to a good approximation, be taken to be equal to those of pure silica. For a PCF, e.g. the strain optic response of silica is completely different from that of air, which is obviously zero for our applications.

To correctly handle a two material fiber one must determine the field energy intensity fraction, f_u, inside the holes of the PCF. The field energy fraction for the base material is then, $1 - f_u$. It is not possible to simply add a contribution, e.g. stress optic, directly to the resonance condition, Eq. (6). Instead every contribution must be weighted with the fraction of field intensity in the corresponding material, as shown in the appendix.

It is possible to make some generalizations about field energy fraction in the holes, f_u, for index guiding fibers. In the short wavelength limit where the wavelength is much smaller than the pitch of the structure, $\lambda \ll \Lambda$, the field is confined to the high index base material. In the long wavelength limit, $\lambda \gg \Lambda$, the changes in the field

are small over a length of the pitch. This imply

$$f_u \to 0 \text{ for } \lambda/\Lambda \to 0, \quad (17)$$
$$f_u \to f \text{ for } \lambda/\Lambda \to \infty, \quad (18)$$

where f is the air filling fraction, i.e. the fraction of area covered by the holes in the cross section of the fiber. The approximation $f_u = 0$ is natural as a first approximation since the field intensity in the air holes f_u is generally much smaller than the field intensity in the base material. But PCFs can possibly have air filling fractions of almost unity, implying that also f_u can be almost unity, and therefore the effect can not be neglected.

We have shown f_u for the FSM in Fig. 6 for air filled holes ($n_h = 1.0$). f_u for the core mode of a PCF with water filled holes ($n_h \simeq 1.33$) is shown in Fig. **??**) and the corresponding FSM is shown in Fig. 6. Clearly f_u is larger for the FSM than for the core mode, and it increases with increasing wavelength and increasing hole diameters d/Λ. The f_u also increases when the index contrast between the hole and base material is decreased. Hence f_u is larger for water filled PCFs than for air filled.

B. Small and large core PCF

In the following we refer to two PCFs to as the large core and the small core PCF. The structure parameters for the small core PCF is $(d/\Lambda, \Lambda) = (0.45, 7\mu m)$ 2) and for the large core PCF $(d/\Lambda, \Lambda) = (0.75, 2\mu m)$. We choose the length of the gratings to be 30 mm for LPGs with additionally $\kappa = 4/L$ for BGs. The sensitivity, γ, is independent of these parameters. The quality factor, Q, depends inversely proportional on the length of the grating, when assuming constant κL. For BGs the quality factor also depends inversely proportional to the coupling constant, κ.

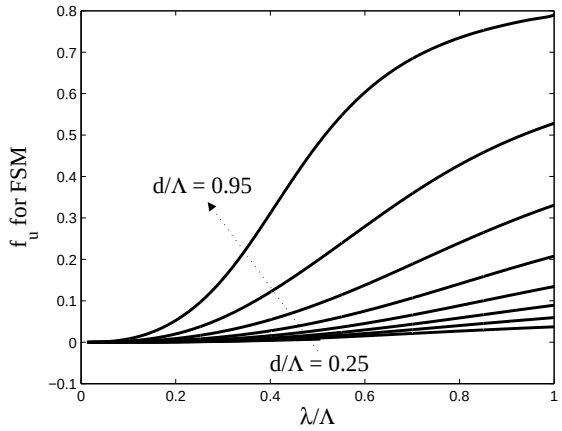

Fig. 6. Field energy intensity fraction in the air filled holes for the fundamental space filling mode. The lines indicate different values of the hole diameter relative to the pitch: 0.15 to 0.95 in steps of 0.10

6. Refractive index sensing and biosensing

A. Refractive index sensing

Refractive index sensors can be used in the application of continuous monitoring of gasses in the oil industry. The gas flows through the PCF is detected by measuring the overall refractive index of the hole contents. Optical fibers have the advantage that there are no electric currents thus avoiding completely the possibility of generating electric sparks.

The sensitivity for refractive index sensing is also used for benchmarking the sensitivity of evanescent wave

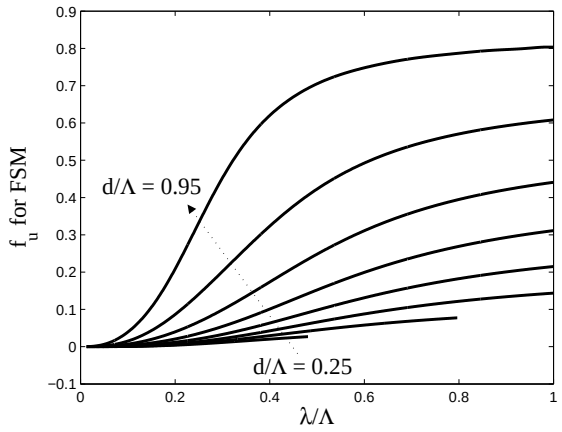

Fig. 7. Field energy intensity fraction in the water filled holes for the fundamental space filling mode. The lines indicate different values of the hole diameter relative to the pitch: 0.15 to 0.95 in steps of 0.10 increasing from below

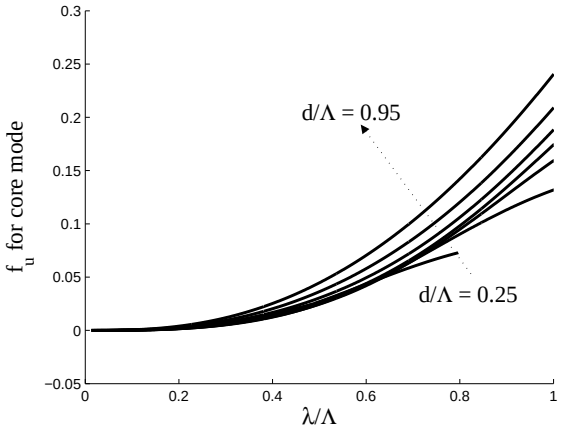

Fig. 8. Field energy intensity fraction in the water filled holes for the core mode. The lines indicate different values of the hole diameter relative to the pitch: 0.15 to 0.95 in steps of 0.10 increasing from below

biosensors, which will be studied in the next section.

Alternatively, a refractive index sensor may be used as tunable grating if the holes are filled with a substance whose refractive index can be controlled[14,19,20]. Tunable gratings may have applications within modulation of optical signals.

Infiltrating substances into PCF-LPGs that are absorbing at the resonant wavelength requires special considerations, as discussed by Daxhelet et al.[31]. In brief the attenuation induced by the absorption of the substance becomes significant if the modes are significantly attenuated over the length of a period of the grating. The interference of modes in the grating becomes weakened and the resonance dip is broadened. Since the grating period of an LPG is much longer than that of a BG, the LPG can be considerably affected by absorbtion, while the BG is largely unaffected even by a high absorbtion.

The change in the effective index of a mode induced by a change of refractive index of the hole contents is proportional to the fraction of the time averaged field energy intensity ($u(\mathbf{r}_\perp) = \frac{1}{2}\varepsilon(\mathbf{r}_\perp)|\mathbf{E}(\mathbf{r}_\perp)|^2$) inside the holes. For BGs the change in $\bar{n}_\mathrm{f} = 2n_\mathrm{co}$ is (see appendix for derivation)

$$\frac{\partial \bar{n}_\mathrm{f}}{\partial n_h} = 2\,\frac{n_\mathrm{g,co}}{n_h} f_{u,\mathrm{co}}, \tag{19}$$

where Δn_h is the change in the refractive index, n_h, of the content in the hole. $f_{u,\mathrm{co}}$ is the fraction of the field energy intensity of the core mode inside the holes. The sensitivity is also proportional to the group index $n_\mathrm{g,co}$. For LPGs the change in $\bar{n}_\mathrm{f} = n_\mathrm{co} - n_\mathrm{cl}$ is

$$\frac{\partial \bar{n}_\mathrm{f}}{\partial n_h} = \frac{n_\mathrm{g,co}}{n_h} f_{u,\mathrm{co}} - \frac{n_\mathrm{g,cl}}{n_h} f_{u,\mathrm{cl}}. \tag{20}$$

It is clear from Eqs. (15,16) that the sensitivity and the detectability are both largely determined by f_u. For BGs f_u should be as large as possible.

For BGs the group index is close to the effective index, $n_\mathrm{g,co} = n_\mathrm{co} - \lambda\partial_\lambda n_\mathrm{co} \approx n_\mathrm{co}$ since the derivative is negligible as seen in Fig. 2. Thus for BGs the sensitivity is determined by $f_{u,\mathrm{co}}$. In Fig. 8 we realize that a large $f_{u,\mathrm{co}}$ implies a small pitch and a large hole diameter. For BGs the size of Q is largely determined by the pitch. Q also increases with decreasing hole size, but to a lesser extent.

In order to have a high Q for LPGs the difference $n_\mathrm{g,co}f_{u,\mathrm{co}} - n_\mathrm{g,cl}f_{u,\mathrm{cl}}$ should be large. Comparing Figs. 8 and 7 we realize that this also implies a small pitch and a large hole diameter. But in this case the difference falls off beyond a certain point in the wavelength pitch ratio. This is because $f_{u,\mathrm{co}}$ and $f_{u,\mathrm{cl}}$ approaches the same limit for large wavelengths, and thus the Q decreases, as seen in Fig. 9.

In Fig. 9 there is also indicated the group index matched line for LPG where $\bar{n}_\mathrm{f} = n_\mathrm{g,co} - n_\mathrm{g,cl} = 0$. Along this line the peak of the LPG is very wide by Eq. (8). On the left side of this line the shift in wavelength are positive for a positive Δn_h. On the right hand side the shift in wavelength is negative for positive Δn_h. The reason for this, is that $\bar{n}_\mathrm{g}$ enters in Eq. (15) in the denominator, and thus its sign determines the sign of the wavelength shift. For BGs group index matching $\bar{n}_\mathrm{f} = 2n_\mathrm{co} - 2\lambda\partial_\lambda n_\mathrm{co} = 0$ does not occur since for the considered index guiding PCFs the effective index is always larger than its derivative.

For the sensitivity of BGs Eq. (19) is inserted in Eq. (15), and plotted for the wavelength 1.0 μm, in Fig. 10. For LPGs Eq. (20) is inserted in the expression for the Q, Eq. (16) and plotted for the wavelength 1.0 μm, Fig. 9.

To give some specific details we choose a typical large mode area, endlessly single mode PCF with structure values: $\Lambda \simeq 7\mu$m and $d/\Lambda \simeq 0.45$. This gives a core diameter of 10 μm. We choose the length of the grating to be 30 mm, and the coupling strength is $\kappa = \pi/(2L)$. We choose different wavelengths for both LPGs and BGs: 600, 900, and 1550 nm. The data is presented in Table 1. The sensitivity increases with increasing wavelength since the evanescent wave is increasing inside the holes, corresponding to an increasing f_u. The sensitivity, γ, for LPGs is four orders of magnitude larger than the sensitivity for BGs. But taking the FWHM of the resonance peak into account, the Q is only slightly larger for LPGs than for BGs.

The data for a small core PCF are presented in Table 1. The small core PCF has significantly higher sensitivity than the large core PCF. Notice that the sensitivity for the small core has opposite sign to the large core PCF. Also Q *decreases* with increasing wavelength. The shift is negative because the PCF's structure parameters places

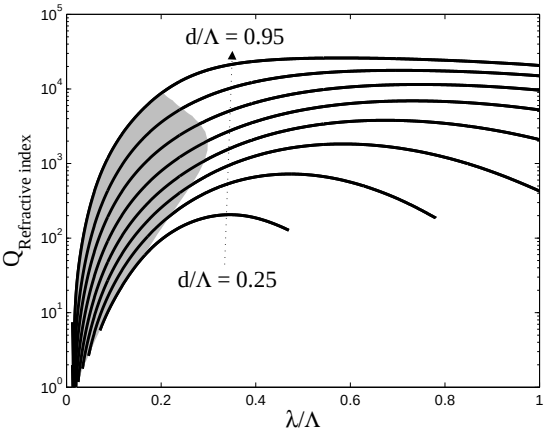

Fig. 9. Quality factor Q_RI for LPG refractive index sensing. The lines indicate different values of the hole diameter relative to the pitch: 0.25 to 0.95 in steps of 0.10. The gray area indicates negative group index mismatch $\bar{n}_\mathrm{g} < 0$. The wavelength is 1 μm, the length of the gratings is $L = 30$ mm, and $|\kappa L| = \pi/(2L)$

large-core PCF	Refractive index sensing			Biosensing			
	$\gamma_{\rm RI}$	$Q_{\rm RI}$	$\Delta\lambda/\Delta n_{\rm h}$ [nm]	$\gamma_{\rm Bio}$ [1/nm]	$Q_{\rm Bio}$ [1/nm]	$\Delta\lambda/t_{\rm Bio}$	$\lambda_{\rm FWHM}$
LPG, 600 nm	1.6	43	980 nm	2.4×10^{3}	63×10^{-3}	1.4 nm/nm	23 nm
LPG, 900 nm	3.2	88	2700 nm	3.0×10^{3}	85×10^{-3}	2.7 nm/nm	32 nm
LPG,1550 nm	14	210	22×10^{3} nm	8.1×10^{-3}	120×10^{-3}	12 nm/nm	109 nm
BG, 600 nm	0.10×10^{-3}	5.8	0.060 nm	3.0×10^{-7}	17×10^{-3}	0.18 pm/nm	10 pm
BG, 900 nm	0.34×10^{-3}	13	0.30 nm	6.5×10^{-7}	25×10^{-3}	0.59 pm/nm	24 pm
BG, 1550 nm	1.6×10^{-3}	35	2.5 nm	19×10^{-7}	41×10^{-3}	2.8 pm/nm	70 pm
small-core PCF	**Refractive index sensing**			**Biosensing**			
	$\gamma_{\rm RI}$	$Q_{\rm RI}$	$\Delta\lambda/\Delta n_{\rm h}$	$\gamma_{\rm Bio}$ [1/nm]	$Q_{\rm Bio}$ [1/nm]	$\Delta\lambda/t_{\rm Bio}$	$\lambda_{\rm FWHM}$
LPG, 600 nm	73	6500	44×10^{3} nm	89×10^{-3}	7.9	-54 nm/nm	6.8 nm
LPG, 900 nm	11	8600	9.8×10^{3} nm	7.7×10^{-3}	6.2	-7.0 nm/nm	1.1 nm
LPG, 1550 nm	6.4	7400	9.9×10^{3} nm	2.7×10^{-3}	3.0	-4.1 nm/nm	1.3 nm
BG, 600 nm	6.0×10^{-3}	350	3.6 nm	17×10^{-6}	1.0	10 pm/nm	10 pm
BG, 900 nm	18×10^{-3}	690	16 nm	35×10^{-6}	1.33	31 pm/nm	23 pm
BG, 1550 nm	74×10^{-3}	1700	115 nm	83×10^{-6}	1.9	130 pm/nm	70 pm

Table 1. Comparison of sensitivity and the quality factor for PCF biosensors and refractive index sensors for both LPGs and BGs at different wavelengths for two different PCFs: a large core of 10 μm and a small core PCF of 1.5 μm.

the PCF on the left of the group index matching line $\bar{n}_{\rm g}=0$ indicated in Fig. 9.

The minimum detectable change in refractive index for LPGs can be calculated. For L = 30 mm, we get a maximal $Q\sim10^4$. Taking that the minimal detectable wavelength is $\lambda_{\rm FWHM}/100$ we get a maximal sensitivity of $\Delta n_{\rm h,min}=\frac{1}{100}\frac{1}{Q}\sim10^{-6}$. The same calculation for a BG with $Q\sim10^2$ gives $\Delta n_{\rm h,min}\sim10^{-4}$.

Both LPGs[20] and BGs[21] have been used for measuring the refractive index of a liquid analyte inside the holes of the PCF. Comparing with experiment for LPGs[20] the PCF has parameters $d/\Lambda=0.47,\Lambda=7.2\mu$m, and the LPG has $\lambda_{\rm r}\simeq845$nm and $L=18.2$ mm. The minimal detectable wavelength shift is $\Delta\lambda_{\rm min}\approx1$ nm. Theoretically the parameters give $Q_{\rm RI}=52$ (no units) and $\lambda_{\rm FWHM}\simeq45$ nm which agrees with the experimental value $\lambda_{\rm FWHM}\approx45$ nm. The minimal sensitivity given the mentioned minimal detectable wavelength is theoretically $\Delta n_{\rm h,min}\approx4.3\times10^{-3}$ which is in agreement with the experimental value $\Delta n_{\rm h,min}\approx10^{-4}$. The shift in resonances wavelength as function of sensitivity is experimentally $\Delta\lambda_{\rm r}/\Delta n_{\rm h}=7500$ nm but gives theoretically a lower value $\Delta\lambda_{\rm r}/\Delta n_{\rm h}=2300$ nm.

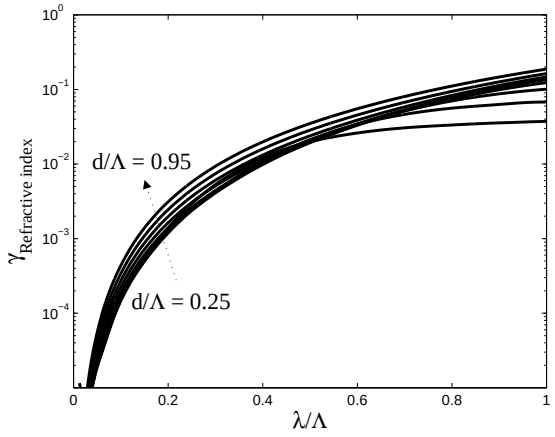

Fig. 10. $\gamma_{\rm RI}$ for BG refractive index sensing. The lines indicate different values of the hole diameter relative to the pitch: 0.15 to 0.95 in steps of 0.10. The wavelength is 1 μm, the length of the gratings is $L=30$ mm, and $|\kappa L|=4$

For BGs we compare with Huy et al.[21]. They have a 6 hole fiber with $d\approx15$ μm and pitch ≈15.8 μm. This gives theoretically $\lambda_{\rm FWHM}\simeq117$ pm in agreement with the experimental $\lambda_{\rm FWHM}\approx150$ pm. Theoretically we have $\Delta\lambda_{\rm r}/\Delta n_{\rm h}\approx0.59$ nm and taking their a minimal detectable wavelength shift of $\Delta\lambda_{\rm min}=1.0$ pm, we find $\Delta n_{\rm h,min}\approx1.7\times10^{-3}$ which is in agreement with the experimental value $\Delta n_{\rm h,min}\approx4\times10^{-3}$. Their numerical simulations gives a minimal detectable shift which is a magnitude off the experimental value.

B. Label-free biosensor

Biosensors in PCFs have seen some interesting developments in recent times. The PCF biosensors can be made to detect both DNA, antibodies or antigens, and the PCF can be made of both silica and polymer materials. The experiments have been conducted using labeled molecules, i.e. target biomolecules have a fluorescent tag, that can be detected using fluorescence or absorbance microscopy. To be really interesting the measurements must be label-free. This can be done with PCF-LPG using the evanescent-wave sensing principle. This principle is used in the widespread surface-plasmon resonance biomolecule interaction analysis instruments.

The evanescent-wave principle measures the increase of refractive index at a surface due to the presence of biomolecules. The experiments are typically carried out in an aqueous environment. Water has refractive index ~ 1.33 and biomolecules have $\sim 1.45 - 1.48$. A given biomolecule may be tested for its affinity to another biomolecule, by immobilizing the first biomolecule onto the surface (functionalization), and then infiltrating the second molecule into the PCF. By a wash any biomolecules that have not been immobilized may be flushed out. The immobilized biomolecules will constitute an increase in the layer of molecules on the surface. The layer is 1-10 nm thick depending on the application.

The film of molecules on the surface may not constitute a homogeneous layer. But since the wavelength is much longer than the thickness of the layer (1 micron $\gg$ 10 nm), the sensor measures the thickness of the biofilm *on average*. The sensor is thus largely insensitive to inhomogeneous distributions of molecules on the surface. For benchmarking we assume that the layer of molecules has a homogeneous thickness $t_{\rm Bio}$ and has a refractive index of 1.45. This refractive index is to a good approximation identical to silica: $n_{\rm r,Bio} \simeq n_{\rm SiO_2}$. Thus a layer of biomolecues $t_{\rm Bio}$ thick corresponds to decrease of $\Delta d = -t_{\rm Bio}/2$ in the hole diameter. To calculate the change in effective index due to a layer of molecules we thus find

$$\frac{\partial n_{\rm eff}}{\partial t_{\rm Bio}} = -2\frac{\partial n_{\rm eff}}{\partial d}, \tag{21}$$

where d is the hole diameter. The change in $\bar{n}_{\rm f}$ for LPGs and BGs is

$$\frac{\partial \bar{n}_{\rm f}}{\partial t_{\rm Bio}} = \begin{cases} -2\left(\frac{\partial n_{\rm co}}{\partial d} - \frac{\partial n_{\rm cl}}{\partial d}\right), & \text{LPG}, \\ -4\frac{\partial n_{\rm co}}{\partial d}, & \text{BG}. \end{cases} \tag{22}$$

In Figs. 11 and 12 it is seen that $Q_{\rm Bio}$ and $\gamma_{\rm Bio}$ are largest for small pitches and large wavelengths. For BGs the $\gamma_{\rm Bio}$ is largely governed by the pitch. For LPGs a large benefit comes from using large holes instead of small holes, whereas the pitch is less important.

For BGs Eq. (22) is inserted in the expression for the sensitivity, Eq. (15) and plotted for the wavelength 1.0 μm, Fig. 12. For LPGs Eq. (22) is inserted in the expression for the Q, Eq. (16) and plotted for the wavelength 1.0 μm, Fig. 11.

To compare with experiments we take the PCF structural values from[20]: $d/\Lambda = 0.47$, $\Lambda = 7.2\mu m$. The wavelength was ≈ 845 nm. This gives $\Delta\lambda = 2.3 \times t_{\rm Bio}$, $Q = 53 \times 10^{-3}$ (no units), and $\gamma = 2.8 \times 10^{-3}$/nm. Thus a 1 nm thick layer of biomolecules gives a 2.3 nm shift in resonant wavelength. It should be noted that the paper[20] gives a value (1.4 nm/nm) that is $\sim 50\%$ more. This is because the effective indices were calculated using a different numerical method, and material dispersion was not included in the simulations.

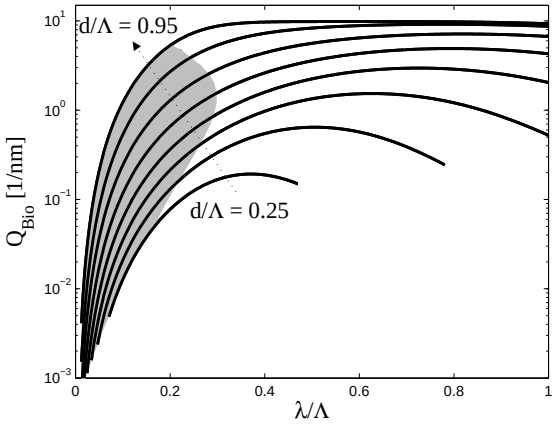

Fig. 11. Quality factor, $Q_{\rm Bio}$, for LPG biosensing. The lines indicate different values of the hole diameter relative to the pitch: 0.25 to 0.95 in steps of 0.10. The gray area indicates negative group index mismatch $\bar{n}_{\rm g} < 0$. The wavelength is 1 μm, the length of the gratings is $L = 30$ mm, and $|\kappa L| = \pi/(2L)$

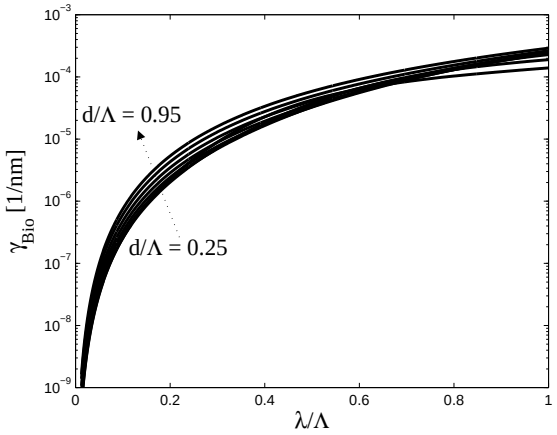

Fig. 12. Sensitivity, $\gamma_{\rm Bio}$, for BG biosensing. The lines indicate different values of the hole diameter relative to the pitch: 0.15 to 0.95 in steps of 0.10. The wavelength is 1 μm, the length of the gratings is $L = 30$ mm, and $|\kappa L| = 4$

In comparison the 6 holes PCF of Huy et al.[21] (d $\approx$ 15 μm, pitch $\approx$ 15.8μm) gives $\Delta\lambda = 0.73 \times 10^{-3} \times t_{\rm Bio}$, $Q = 6.2 \times 10^{-3}$/nm, and $\gamma = 0.47 \times 10^{-6}$/nm at $\lambda_{\rm r} \simeq$ 1555nm. Thus a 1 nm thick layer of biomolecules gives a 0.73 pm shift in resonant wavelength.

In general, both the sensitivity and the quality factor for BGs is monotonically increasing with increasing wavelength. They also increase with increasing hole size as seen in Table 1. The general behavior for the both the sensitivity and the quality factor for LPGs is more complicated. The sensitivity is strongly influenced by the group index matching, and the resonant wavelength shifts can change sign depending on the PCF structure parameters. The quality factor, Q, is high for large air holes, and big normalized wavelength λ/Λ.

In conclusion, the sensitivity of label-free PCF grating biosensors follows roughly the tendencies of the refractive index sensors. The sensitivity varies several orders of magnitude in sensitivity and quality factor with the PCF structure parameter. BGs have a high sensitivity when the pitch is small compared with the wavelength. Thus the optimal BG biosensor sensor is a small core fiber. For LPGs the quality factor is high when the air holes are large, and are less influenced by wavelength to pitch ratio, except in the short limit where the quality goes to zero. The optimal LPG biosensor or refractive index sensor thus has very large holes and a pitch about three times or less the wavelength.

7. Temperature and strain sensing

A. *Temperature*

Sensitivity to temperature is often an unwanted source of error in fiber gratings. However, fiber gratings may also be employed as high temperature sensors since silica is stable to high temperatures. If the susceptibility to temperature is an unwanted effect it may also be remedied by using two multiplexed fiber gratings each with a different linear temperature response. In the following we will study the temperature response of air filled silica PCFs although the theory is also applicable to other materials.

Temperature changes both the material refractive indices of the PCF through the thermo-optic effect and also by expansion of the PCF structure. The thermo-optic coefficient for the refractive indexof silica glass is $C_T^n \simeq 9 \times 10^{-6}$/K and the thermal expansion coefficient is $\alpha \simeq 0.55 \times 10^{-6}$/K. Since the perturbation of the PCF is sufficiently small we may expand the effective index to first order in the temperature. Since both the pitch, length and the refractive index of the silica are dependent on silica, we use the partial derivatives of the effective refractive index (the chain rule)

$$\begin{aligned}\frac{\partial n_{\rm eff}}{\partial T}\Big|_{\lambda_{\rm r}} &= \frac{{\rm d}n_{\rm eff}\big(L(T),\Lambda(T),n_r(T)\big)}{{\rm d}T} \\ &= \frac{\partial n_{\rm eff}}{\partial L}\frac{\partial L}{\partial T} + \frac{\partial n_{\rm eff}}{\partial \Lambda}\frac{\partial \Lambda}{\partial T} + \frac{\partial n_{\rm eff}}{\partial n_{\rm b}}\frac{\partial n_{\rm b}}{\partial T}.\end{aligned} \tag{23}$$

We readily identify the thermal expansion $\frac{\partial \Lambda}{\partial T} = \alpha\Lambda$ and $\frac{\partial L}{\partial T} = \alpha L$. The partial derivative of the effective index with respect to the length can be evaluated according to following argumentation. An elongated PCF at a fixed effective index is equivalent to a PCF at fixed length with an increased effective index. Formulated in mathematical terms this yields

$$\frac{\partial n_{\rm eff}}{\partial L} = \frac{n_{\rm eff}}{L}. \tag{24}$$

In Eq. (23) the partial derivative of the effective index with respect to the pitch (2nd term rhs) must be evaluated numerically. The contribution from the thermo-optic effect can be evaluated using Eq. (36). Eq. (23) can then be written for a BG as

$$\frac{\partial \bar{n}_{\rm f}}{\partial T}\Big|_{\lambda_{\rm r}} = 2\alpha\big(n_{\rm co} + \Lambda\frac{\partial n_{\rm co}}{\partial \Lambda}\big) + \frac{C_T^n}{n_{\rm b}}(1-f_{\rm u,co})n_{\rm g,co} \tag{25}$$

For an LPG we get

$$\begin{aligned}\frac{\partial \bar{n}_{\rm f}}{\partial T}\Big|_{\lambda_{\rm r}} &= \alpha\big(\bar{n}_{\rm f} + \Lambda\frac{\partial \bar{n}_{\rm f}}{\partial \Lambda}\big) \\ &\quad + \frac{C^n_{{\rm b},T}}{n_{\rm b}}\big[(1-f_{u,{\rm co}})n_{\rm g,co} - (1-f_{u,{\rm cl}})n_{\rm g,cl}\big].\end{aligned} \tag{26}$$

For generality we have kept a general refractive index of the base material.

For BGs Eq. (25) is inserted in the expression for the sensitivity, Eq. (15), and plotted for the wavelength 1.0 μm, Fig. 14. For LPGs Eq. (26) is inserted in the expression for the Q, Eq. (16), and plotted for the wavelength 1.0 μm in Fig. 13.

The sensitivity of BG PCF temperature sensors is almost constant for the structure parameters, Λ and d/Λ, Fig. 14. The Q value for PCF-LPG temperature sensors in contrast varies several orders of magnitude with the structure parameters, Λ and d/Λ, Fig. 13. The dips seen on the left in the figures is a change of sign of the wavelength shift.

In table 2 we see that the resonant wavelength shifts for both BGs and LPGs are of the order of 5pm/K, regardless of PCF parameters. The quality factor is several orders of magnitude smaller for LPGs compared with BGs. This can be attributed to the a partial cancelation of the thermo-optic terms of the core and cladding mode in Eq. (26).

We note that the sensitivities for the BGs are surprisingly constant in Table 2. In the rhs of Eqs. (26, 25) the terms $n_{\rm eff} + \Lambda\frac{\partial n_{\rm eff}}{\partial \Lambda}$ and $n_{\rm g}(1-f_u)/n_b$ are roughly

of the same order of magnitude. The prefactor for the thermo-optic term is larger than the prefactoc of thermal expansion term, $C_n^T/\alpha \approx 20$. The temperature response of the grating is largely determined by the thermo-optic. For BGs we may thus approximate $\gamma_T = 1/\lambda \frac{\partial \lambda_\mathrm{r}}{\partial T} = C_n^T/n_\mathrm{b}\Delta T$. For silica PCFs $\gamma_T \simeq C_n^T/n_\mathrm{b} \simeq 0.62\times 10.6/\mathrm{K}$ in good agreement with the values given in tables 2 and 2. We conclude that sensitivity of BG temperature sensors is constant, within a few % margin, for all PCF structures and is dominated by the thermo-optic coefficient relative to the refractive index of the base material.

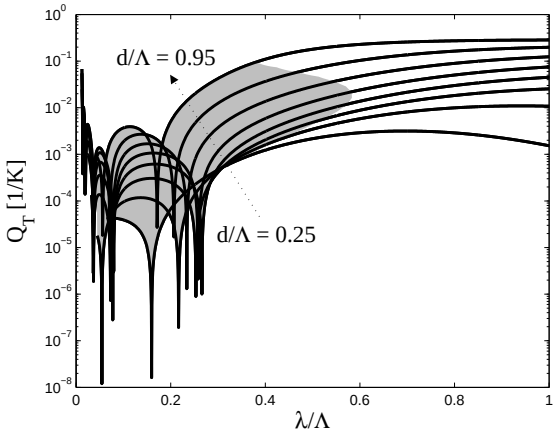

Fig. 13. Quality factor, Q_T, for LPG temperature sensing. The lines indicate different values of the hole diameter relative to the pitch: 0.25 to 0.95 in steps of 0.10. The gray area indicates negative group index mismatch $\bar{n}_\mathrm{g} < 0$. The wavelength is 1 μm, the length of the gratings is $L = 30$ mm, and $|\kappa L| = \pi/(2L)$

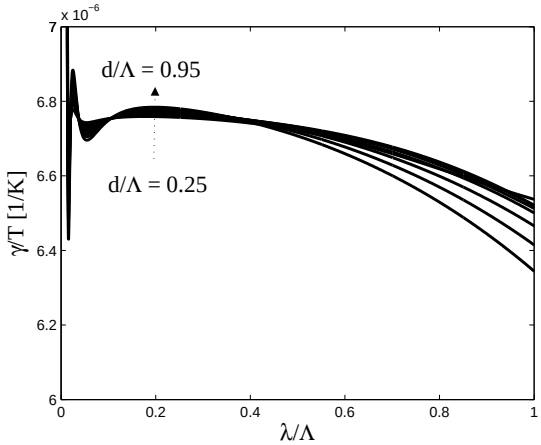

Fig. 14. Sensitivity, γ_T, for BG temperature sensing. The lines indicate different values of the hole diameter relative to the pitch: 0.15 to 0.95 in steps of 0.10. The wavelength is 1 μm, the length of the gratings is $L = 30$ mm, and $|\kappa L| = 4$

To validate our theory we compare with experiments. Dobb et al.[32] characterized LPGs in PCFs inscribed with an electric arc. For a PCF with structure parameters $\Lambda \simeq 7.1$ μm, $d \simeq 4.0 \pm 0.4$ μm they found a shift of resonance wavelength with temperature as 3.4 pm/K at the wavelength 1511 nm. Using the structure parameters in the theory yields 4.3 pm/K. For a PCF with structure parameters $\Lambda \simeq 8$ μm, $d \simeq 3.7\mu$m, they found 2.2 pm/K at 1403 nm wavelength and the theory gives 6.1 pm/K. Thus we have an agreement of the right magnitude and right sign of the wavelength shift. It is seen in Fig. 14 that for their structure values, $d/\Lambda \simeq 0.46, \lambda/\Lambda \simeq 0.18$ the quality factor, Q, experiences a series of dips. The dips correspond to the terms in Eq. (26) cancel in the net contribution. Both numerically, and experimentally, an estimation of the sensitivity will be prone to small errors on contribution from each term.

In an earlier experiment Humbert et al.[4] used the electric arc method to inscribe LPGs in a PCF with structure parameters $\Lambda \simeq 4.0\mu$m, $d \simeq 2.0\mu$m. They found a value of 9 pm/K at 1590 nm, roughly half the theoretical value -23 pm/K, but with an opposite sign. To inscribe BGs Martelli et al. used a PCF with a erbium-doped UV sensitive core[33]. Their structure parameters are roughly $\Lambda \simeq 10\mu$m, $d \simeq 2\mu$m. At a wavelength of 1535 nm the wavelength shift is 20 pm/K. The theory gives 10 pm/K for a pure silica PCF. An erbium doped core is known to decrease the temperature sensitivity in standard optical fibers.

BGs have also been inscribed in a small core fiber with the structure parameters $d/\Lambda = 0.5$ and $\Lambda = 1.6\mu$m[12]. The core was doped with germanium to make the core UV-sensitive. They found an experimental sensitivity of 4.11 pm/K at a wavelength of 1508 nm. Our theory gives 9.9 pm/K. A Germanium doped core is known to decrease the temperature sensitivity in standard optical fibers.

To enhance the temperature sensitivity in PCF the holes can be filled with substances with a high thermo-optic coefficient. This has been shown to increase temperature sensitivity[14]. Eq. (26) can in this case be modified to be valid by adding an additional temperature optic term for the holes.

large-core PCF	Temperature			Strain			
	$\gamma_{\rm T}$	$Q_{\rm T}$ [1/K]	$\Delta\lambda/\Delta T$ [1/K]	γ_{ε_s}	Q_{ε_s}	$\Delta\lambda/\varepsilon_s$	$\lambda_{\rm FWHM}$
LPG, 600 nm	3.9×10^{-6}	14×10^{-5}	2.3 pm	-1.2×10^{-6}	4.5×10^{-5}	-0.74 pm	17 nm
LPG, 900 nm	6.2×10^{-6}	30×10^{-5}	5.6 pm	-2.3×10^{-6}	11×10^{-5}	-2.1 pm	19 nm
LPG, 1550 nm	1.7×10^{-6}	10×10^{-5}	27 pm	-2.1×10^{-6}	13×10^{-5}	-3.3 pm	26 nm
BG, 600 nm	6.7×10^{-6}	0.39	4.0 pm	0.82×10^{-6}	0.047	0.49 pm	10 pm
BG, 900 nm	6.8×10^{-6}	0.26	6.1 pm	0.82×10^{-6}	0.031	0.73 pm	24 pm
BG, 1550 nm	6.8×10^{-6}	0.15	11 pm	0.81×10^{-6}	0.018	1.3 pm	70 pm
small-core PCF	**Temperature**			**Strain**			
	$\gamma_{\rm T}$	$Q_{\rm T}$ [1/K]	$\Delta\lambda/\Delta T$ [1/K]	γ_{ε_s}	Q_{ε_s}	$\Delta\lambda/\varepsilon_s$	$\lambda_{\rm FWHM}$
LPG, 600 nm	5.0×10^{-5}	5.8×10^{-3}	-3.0 pm	-2.4×10^{-6}	2.8×10^{-3}	-1.4 pm	0.52 nm
LPG, 900 nm	4.0×10^{-5}	23×10^{-3}	-36 pm	-4.2×10^{-6}	2.4×10^{-3}	-2.0 pm	1.6 nm
LPG, 1550 nm	3.7×10^{-5}	55×10^{-3}	57 pm	0.7×10^{-6}	1.0×10^{-3}	1.1 pm	1.0 nm
BG, 600 nm	6.7×10^{-6}	0.39	4.0 pm	0.81×10^{-6}	0.047	0.48 pm	10 pm
BG, 900 nm	6.7×10^{-6}	0.26	6.1 pm	0.79×10^{-6}	0.030	0.71 pm	23 pm
BG, 1550 nm	6.6×10^{-6}	0.15	10 pm	0.75×10^{-6}	0.017	1.2 pm	68 pm

Table 2. Comparison of sensitivity and the quality factor for PCF temperature and strain sensors for both LPGs and BGs at different wavelengths for two different PCFs: a large core of 10 μm and a small core PCF of 1.5 μm

B. Strain

Fiber optic strain sensors have found application within civil engineering, where they provide a stable and sensitive measurement of the strain in constructions. Strain is defined as the relative elongation: $\varepsilon_s = \Delta L/L$ of a piece PCF of length L. Often millistrain, $\mu\varepsilon_s = 10^6\varepsilon$, is used instead of strain. When the PCF is elongated, the PCF contracts transversely to the applied strain. This is expressed by Poisson's ratio which formally is the ratio between lateral and tensile strain with a negative sign. For silica glass Poisson's ratio is given by $\nu = 0.17$. Strain also changes the refractive index of materials. The strain-optic coefficient for silica is $C_\epsilon^n = \eta_\epsilon = -0.26$[34]. Since strain changes the length, pitch, and the material refractive indices we apply partial derivatives (the chain rule) to the linearization of the effective index

$$\begin{aligned}\frac{\partial n_{\rm eff}}{\partial\varepsilon_s}\Big|_{\lambda_{\rm r}} &= \frac{{\rm d}n_{\rm eff}\big(L(\varepsilon_s),\Lambda(\varepsilon_s),n_r(\varepsilon_s)\big)}{{\rm d}\varepsilon_s}\\ &= \frac{\partial n_{\rm eff}}{\partial L}\frac{\partial L}{\partial\varepsilon_s}+\frac{\partial n_{\rm eff}}{\partial\Lambda}\frac{\partial\Lambda}{\partial\varepsilon_s}+\frac{\partial n_{\rm eff}}{\partial n_r}\frac{\partial n_r}{\partial\varepsilon_s}.\end{aligned} \tag{27}$$

Since $L(\varepsilon_s) = (1+\varepsilon_s)L$ we have $\frac{\partial L}{\partial\varepsilon_s} = L$ and $\Lambda(\varepsilon_s) = (1+\varepsilon_s)\Lambda$ gives $\frac{\partial\Lambda}{\partial\varepsilon_s} = -\nu\Lambda$. An increase in length of the PCF with a fixed effective index is mathematically equivalent to a fixed length with an increase in effective index,

$$\frac{\partial n_{\rm eff}}{\partial L} = \frac{n_{\rm eff}}{L}. \tag{28}$$

The derivative of the effective index with respect to the refractive index of the base material may be evaluated by inserting the strain-optic coefficient in the perturbative formula, Eq. (36), given in the appendix. The formula for BGs is

$$\begin{aligned}\frac{\partial n_{\rm f}}{\partial\varepsilon_s}\Big|_{\lambda_{\rm r}} &= 2n_{\rm co}-\nu\Lambda\frac{\partial 2n_{\rm co}}{\partial\Lambda}\\ &\quad+\frac{\eta_\varepsilon}{n_b}2n_{\rm g,co}(1-f_{u,{\rm co}}),\end{aligned} \tag{29}$$

while for LPGs we obtain

$$\begin{aligned}\frac{\partial\bar n_{\rm f}}{\partial\varepsilon_s}\Big|_{\lambda_{\rm r}} &= (n_{\rm co}-n_{\rm cl})-\nu\Lambda\frac{\partial(n_{\rm co}-n_{\rm cl})}{\partial\Lambda}\\ &\quad+\frac{\eta_\varepsilon}{n_b}\big(n_{\rm g,co}(1-f_{u,{\rm co}})-n_{\rm g,cl}(1-f_{u,{\rm cl}})\big).\end{aligned} \tag{30}$$

Eqs. (29,30) are inserted in the expression for the sensitivity, Eq. (15) and calculated for the wavelength 1.0 μm. The results are shown in Figs. 16 and **??**, respectively. The sensitivity for BGs is very close to being constant regardless of pitch, hole diameters, and wavelength, as seen in Fig. 16 and Table 2. This can understood by that fact that $n_{\rm co}$ and $n_{\rm g,co}$ are of similar magnitudes, such that $n_{\rm co} \gg \Lambda\frac{\partial n_{\rm co}}{\partial\Lambda}$. We can neglect the second term in Eq. 29. We then put $\Delta\bar n_{\rm f}/\varepsilon_s = (1+\eta_\varepsilon/n_b)n_{\rm g,co} \simeq 0.8\times n_{\rm g,co}$, where $n_b \simeq 1.45$ is the refractive index of silica. Inserting this in the expression for the sensitivity, Eq. (15), we realize that $\gamma_{\varepsilon_s}/\mu\varepsilon_s \approx 0.8\times10^{-6}$ and $\Delta\lambda = 0.8\times10^{-6}\,\lambda\,\mu\varepsilon_s$. This result is in very good agreement with the values for BGs displayed in table 2 and in Fig. 16.

The quality factor, Q_{ε_s}, for LPGs with $\lambda/\Lambda > 0.2$ tends to increase for increasing hole size, while being almost independent of wavelength, as seen in Fig. 15. For these wavelength the first term in Eq. (30), the elongation of the PCF, is dominating over the strain-optic effect and the lateral strain. For $\lambda/\Lambda < 0.2$ the sensitivity is generally lower since $\bar{n}_{\rm f}$ decrease for decreasing wavelengths, but also because the strain-optic effect and the lateral strain become significant. The dips indicate a net cancelation of the terms in Eq. (30).

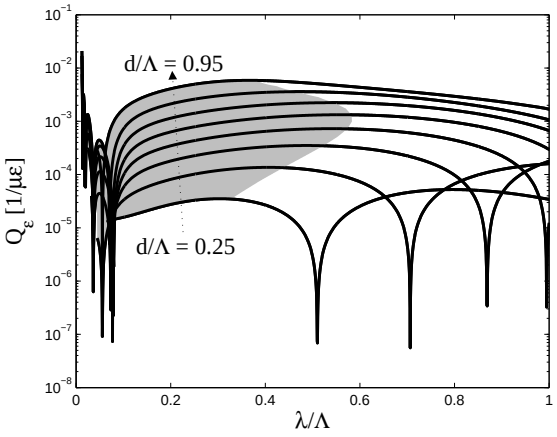

Fig. 15. Quality factor, Q_{ε_s}, for LPG strain sensing. The lines indicate different values of the hole diameter relative to the pitch: 0.25 to 0.95 in steps of 0.10. The gray area indicates negative group index mismatch $\bar{n}_{\rm g} < 0$. The wavelength is 1 μm, the length of the gratings is $L = 30$ mm, and $|\kappa L| = \pi/(2L)$

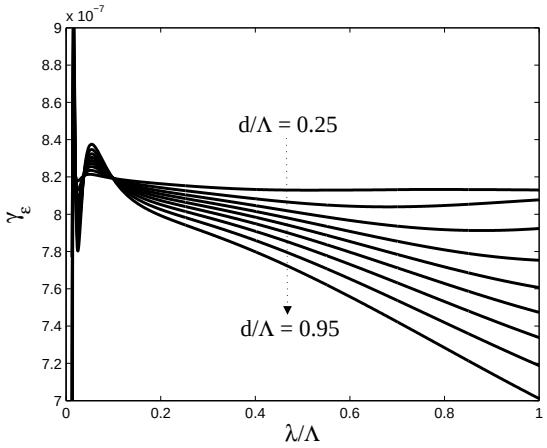

Fig. 16. Sensitivity ,γ_{ε_s}, for BG strain sensing. The lines indicate different values of the hole diameter relative to the pitch: 0.15 to 0.95 in steps of 0.10. The wavelength is 1 μm, the length of the gratings is $L = 30$ mm, and $|\kappa L| = 4$

To validate our theory we compare with experiments. Dobb et al.[32] characterized LPGs in PCFs inscribed with an electric arc. For a PCF with structure parameters $\Lambda \simeq 7.1\mu$m, $d \simeq 4.0\mu$m they found a shift of resonance wavelength with -2.5 pm/$\mu\varepsilon_s$ at the wavelength 1688 nm. Using the structure parameters in the theory yields -3.7 pm/$\mu\varepsilon_s$. For a PCF with structure parameters $\Lambda \simeq 8\mu$m, $d \simeq 3.7\mu$m, they found -2.08/$\mu\varepsilon_s$ at 1403 nm wavelength and the theory gives -3.2/$\mu\varepsilon_s$. Thus we have an agreement of the right magnitude and right sign of the wavelength shift. Their PCF structure values, $d/\Lambda \simeq 0.46, \lambda/\Lambda \simeq 0.18$, gives a Q that is close to the dips in Fig. 15. The dips corresponds to a cancelation of the terms in Eq. (30) and close to the dips the quality factor is more susceptible to errors between experimental and numerical parameters. Martelli et al. used a PCF with a erbium-doped UV sensitive core to inscribe BGs[33]. Their structure parameters are roughly $\Lambda \simeq 10\mu$m, $d \simeq 2\mu$m. At a wavelength of 1535 nm the wavelength shift is 1.2 pm/$\mu\varepsilon_s$. The theory gives 1.25 pm/$\mu\varepsilon_s$ for a pure silica PCF. A doped core does not change the strain-optic coefficient significantly due to a doped core[34].

For BGs in a small core fiber with the structure parameters $d/\Lambda \simeq 0.5$ and $\Lambda \simeq 1.6\mu$m[12] it is found experimentally a sensitivity of 1.25 pm/$\mu\varepsilon$ at the wavelength 1508 nm. The core was doped with germanium to make the core UV-sensitive. Our theory gives 1.16 pm/$\mu\varepsilon$ in good agreement with the experimental value.

In conclusion we have found that the sensitivity for BGs is approximately constant both for temperature and strain sensing, with the coefficients $\gamma_T \simeq 0.62 \times 10.6$/K and $\gamma_{\mu\varepsilon_s} \simeq 0.8 \times 10^{-6}$ for pure silica PCFs. The wavelength shift both for BGs and LPGs is generally of the order of 5 pm/K, and the sensitivity and quality factor are an order of magnitude large (in K) compared with strain (in microstrain). The quality factor for LPGs for temperature and strain sensing has roughly the same characteristics.

8. Conclusion

In conclusion we have shown that the performance of LPG sensors are best characterized by the detectability, Q, rather than the sensitivity, γ. We have calculated expressions for the sensitivity, that incorporates the material-optic responses to the external perturbation, as well as treated effects of having air holes in the structure. Using the results of a fully-vectorial finite element calculations, incorporating material dispersion, the sensitivity and detectability have been calculated for a range of PCF structure parameters, i.e. hole diameters and pitch lengths.

We have proposed expressions for the sensitivity for internal refractive index sensing, label-free biosensing, strain, and temperature sensing. For strain and temperature we have included both thermo-optic and strain-optic effects, as wells as the effects of both longitudinal and lateral elongation. The formulas are of general form

and apply to all PCFs as well as standard optical optical fibers.

For PCFs infiltrated with samples, the Q for refractive index sensing and biosensing may be improved by several orders of magnitude by appropriate choice of the hole size and pitch. For temperature and strain index sensing with BG sensors we have shown that the sensitivity is almost constant for all PCFs. For LPGs an accurate theoretical prediction of the sensitivity for temperature sensing or strain sensing can be difficult since the sensitivity strongly affected by the waveguide dispersion. However, our analysis shows that the low temperature sensitivity of PCF-gratings, ∼5 pm/K, is generally valid for all PCFs.

L. Rindorf's e-mail address is lhr@com.dtu.dk.

9. Appendix: First order perturbation theory

The linear change in propagation constant by a small perturbation in the dielectric function, $\Delta\varepsilon$, is[35]

$$\Delta\beta_m = \frac{\omega}{2}\frac{\partial\beta}{\partial\omega}\frac{\int_\Omega d\mathbf{r}_\perp \Delta\varepsilon(\mathbf{r}_\perp)|\mathbf{E}_m(\mathbf{r}_\perp)|^2}{\int_\Omega d\mathbf{r}_\perp \varepsilon(\mathbf{r}_\perp)|\mathbf{E}_m(\mathbf{r}_\perp)|^2}. \quad (31)$$

Ω denotes the fiber cross section. By setting the norm of the orthogonal solutions to the Helmholtz equation (1) to unity,

$$\int_\Omega \mathrm{d}\mathbf{r}_\perp \mathbf{E}_m^\dagger(\mathbf{r}_\perp)\varepsilon(\mathbf{r}_\perp)\mathbf{E}_n(\mathbf{r}_\perp) = \delta_{mn}, \quad (32)$$

where † denotes Hermitian conjugate (the complex conjugate transposed), we get

$$\Delta n_{textrmeff,m} = \frac{n_{\mathrm{g},m}}{2}\int_\Omega \mathrm{d}\mathbf{r}_\perp \Delta\varepsilon(\mathbf{r}_\perp)|\mathbf{E}_m(\mathbf{r}_\perp)|^2 \quad (33)$$

with the group index, $n_{\mathrm{g},m} \equiv \mathrm{c}\frac{\partial\beta}{\partial\omega}$. We define the field energy intensity in the air holes of the mode m by

$$f_{u,m} \equiv \frac{\int_{\Omega_\mathrm{h}} d\mathbf{r}_\perp \mathbf{D}_m^\dagger(\mathbf{r}_\perp)\cdot\mathbf{E}_m(\mathbf{r}_\perp)}{\int_\Omega d\mathbf{r}_\perp \mathbf{D}_m^\dagger(\mathbf{r}_\perp)\cdot\mathbf{E}_m(\mathbf{r}_\perp)}. \quad (34)$$

Ω_h is the part of the fiber cross section covering holes, and $\mathbf{D} = \varepsilon\mathbf{E}$. The linear change in effective index of mode m caused by a change of the refractive index of the holes is then

$$\frac{\partial n_{\mathrm{eff},m}}{\partial n_\mathrm{h}} = \frac{n_{\mathrm{g},m}}{n_\mathrm{h}} f_{u,m} \quad (35)$$

where n_h is the refractive index of the holes. The change is proportional to $f_{u,m}$ The corresponding linear change in effective index caused by a change of the refractive index of the base material is

$$\frac{\partial n_{\mathrm{eff},m}}{\partial n_\mathrm{b}} = \frac{n_{\mathrm{g},m}}{n_\mathrm{b}}(1 - f_{u,m}) \quad (36)$$

where n_b is the refractive index of the base material. It is seen that the change is proportional to the field intensity in the base material, $1 - f_u$.

References

1. B. Lee, "Review of the present status of optical fiber sensors," Optical Fiber Technology **9**, 57–79 (2003).
2. T. A. Birks, J. C. Knight, and P. S. J. Russell, "Endlessly single mode photonic crystal fibre," Opt. Lett. **22**, 961–963 (1997).
3. M. A. van Eijkelenborg, M. C. J. Large, A. Argyros, J. Zagari, S. Manos, N. Issa, I. Bassett, S. Fleming, R. C. McPhedran, C. M. de Sterke, and N. A. P. Nicorovici, "Microstructured polymer optical fibre," Opt. Express **9**, 319 – 327 (2001).
4. G. Humbert, A. Malki, S. Fevrier, P. Roy, and D. Pagnoux, "Electric arc-induced long-period gratings in ge-free air-silica microstructure fibres," Electron. Lett. **4**, 349–350 (2003).
5. G. Kakarantzas, T. A. Birks, and P. S. J. Russell, "Strucural long-period gratings in photonic crystal fibers," Opt. Lett. **27**, 1013–1015 (2002).
6. M. D. Nielsen, G. Vienne, J. R. Folkenberg, and A. Bjarklev, "Investigation of micro deformation induced attenuation spectra in a photonic crystal fiber," Opt. Lett. **28**, 236–238 (2003).
7. B. J. Eggleton, P. S. Westbrook, R. S. Windeler, S. Spälter, and T. A. Strasser, "Grating resonances in air-silica microstructured optical fibers," Opt. Lett. **24**, 1460 – 1462 (1999).
8. G. D. Peng, Z. Xiong, and P. L. Chu, "Photosensitivity and gratings in dye-doped polymer optical fibers," Opt. Fiber. Technol. **5**, 242–251 (1999).
9. Z. Li, Y. Tam, L. Xu, and Q. Zhang, "Fabrication of long-period gratings in poly(methyl methacrylate-co-methyl vinyl ketone-cobenzyl methacrylate)-core polymer optical fiber by use of a mercury lamp," Opt. Lett. **30**, 1117–1119 (2005).
10. H. Dobb, D. Webb, K. Kalli, A. Argyros, M. Large, and M. van Eijkelenborg, "Continuous wave ultraviolet light-induced fiber bragg gratings in few- and single-mode microstructured polymer optical fibers," Opt. Lett. **30**, 3296–3298 (2005).
11. M. P. Hiscocks, M. A. van Eijkelenborg, A. Argysor, and M. C. J. Large, "Stable imprinting of long-period gratings in microstructured polymer optical fibre," Opt. Express **14**, 4644–4649 (2006).
12. O. Frazao, J. P. Carvalho, L. A. Ferreira, F. M. Araujo, and J. L. Santos, "Discrimination of strain and temperature using bragg gratings in microstructured and standard optical fibres," Meas. Sci. Technol. **16**, 2109–2113 (2005).
13. H. Dobb, K. Kalli, and D. Webb, "Temperature-insensitive long period grating sensors in photonic crystal fibre," Electron. Lett. **11**, 657–658 (2004).
14. H. R. Sorensen, J. Canning, J. Laegsgaard, and K. Hansen, "Control of the wavelength dependent thermo-optic coefficients in structured fibres," Opt. Express **14**, 6428–6433 (2006).
15. M. P. DeLisa, Z. Zhang, M. Shiloach, S. Pilevar, C. C. Davis, J. S. Sirkis, and W. E. Bentley,

"Evanescent wave long-period fiber bragg grating as an immobilized antibody biosensor," Analytical Chemistry **72**, 2895–2900 (2000).
16. J. B. Jensen, L. H. Pedersen, P. E. Hoiby, L. B. Nielsen, T. P. Hansen, J. R. Folkenberg, J. Riishede, D. Noordegraaf, K. Nielsen, A. Carlsen, and A. Bjarklev, "Photonic crystal fiber based evanescent-wave sensor for detection of biomolecules in aqueous solutions," Opt. Lett. **29**, 1974–1976 (2004).
17. J. B. Jensen, P. E. Hoiby, G. Emiliyanov, O. Bang, L. H. Pedersen, and A. Bjarklev, "Selective detection of antibodies in microstructured polymer optical fibers," Opt. Express **13**, 5883–5889 (2005).
18. G. Emiliyanov, J. B. Jensen, O. Bang, P. E. Hoiby, L. H. Pedersen, E. M. Kjaer, and L. Lindvold, "Localized biosensing with topas microstructured polymer optical fiber," Opt. Lett. **32**, 460–462 (2007). Opt. Lett. **32**, 1059 (2007).
19. C. Kerbage and B. Eggleton, "Tunable microfluidic optical fiber gratings," **82**, 1338–1340 (2003).
20. L. Rindorf, J. B. Jensen, M. Dufva, L. H. Pedersen, P. E. Hoiby, and O. Bang, "Biochemical sensing using photonic crystal fiber long-period gratings," Opt. Express **14**, 8824–8831 (2006).
21. M. C. P. Huy, G. Laffont, Y. Frignac, V. Dewynter-Marty, P. Ferdinand, P. Roy, J.-M. Blondy, D. Pagnoux, W. Blanc, and B. Dussardier, "Fibre bragg grating photowriting in microstructured optical fibres for refractive index measurement," Meas. Sci. Technol. **17**, 992–997 (2006).
22. L. Rindorf, P. E. Hoiby, J. B. Jensen, L. H. Pedersen, O. Bang, and O. Geschke, "Towards biochips using microstructured optical fiber sensors," Analytical and Bioanalytical Chemistry (2006).
23. B. R. Acharya, T. Krupenkin, S. Ramachandran, Z. Wang, C. C. Huang, and J. A. Rogers, "Tunable optical fiber devices based on broadband long-period gratings and pumped microfluidics," **83**, 4912–4914 (2003).
24. S. Ramachandran, "Dispersion-tailored few-mode fibers: A versatile platform for in-fiber photonic devices," J. Lightwave Technol. **23**, 3426–3443 (2005).
25. B. T. Kuhlmey, R. C. McPhedran, and C. M. de Sterke, "Modal cutoff in microstructured optical fibers," Opt. Lett. **27**, 1684–1686 (2002).
26. N. A. Mortensen, J. R. Folkenberg, M. D. Nielsen, and K. P. Hansen, "Modal cutoff and the v parameter in photonic crystal fibers," Opt. Lett. **28**, 1879–1881 (2003).
27. A. Yariv and P. Yeh, *Photonics* (Oxford University Press, Oxford, 2007).
28. X. W. Shu, L. Zhang, and I. Bennion, "Sensitivity characteristics of long-period fiber gratings," J. Lightwave Technol. **20**, 255–266 (2002).
29. Http://www.comsol.com.
30. Http://www.iapws.org/relguide/rindex.pdf.
31. X. Daxhelet and M. Kulishov, "Theory and practice of long-period gratings: when a loss becomes a gain," Opt. Lett. **28**, 686–688 (2003).
32. H. Dobb, K. Kalli, and D. Webb, "Measured sensitivity of arc-induced long-period grating sensors in photonic crystal fibre," Opt. Com. **260**, 184–191 (2006).
33. C. Martelli, J. Canning, N. Groothoff, and K. Lyytikainen, "Strain and temperature characterization of photonic crystal fiber bragg gratings," Opt. Lett. **30**, 1785–1787 (2005).
34. Y. Park, T.-J. Ahn, Y. H. Kim, W.-T. Han, U.-C. Paek, and D. Y. Kim, "Measurement method for profiling the residual stress and the strain-optic coefficient of an optical fiber," Appl. Opt. **41**, 21–26 (2002).
35. A. W. Snyder and J. D. Love, *Optical Waveguide Theory* (Chapman & Hall, New York, 1983).